

1 **Title:**

2 **Changes in distribution, morphology and ultrastructure of chloride cell in Atlantic**
3 **salmon during an AGD infection**

4

5

6

7 **Short running title:** impact of amoebic gill disease on chloride cells

8

9 Yao-Chung Chang¹, Harry Hamlin-Wright¹, Sean Monaghan¹, Tharangani Herath², Johanna
10 Bailly¹, Jorge del Pozo³, Jamie Downes⁴, Andrew Preston¹, Lynn Chalmers¹, Nilantha
11 Jayasuriya⁵, James E. Bron¹, Alexandra Adams¹ and Sophie Fridman¹

12

13 ¹ Institute of Aquaculture, School of Natural Sciences, University of Stirling, Stirling,
14 Stirlingshire, Scotland, FK9 4LA

15 ² Department of Animal Production, Welfare and Veterinary Sciences, Harper Adams
16 University, Newport, Shropshire, England, TF10 8NB

17 ³ The Royal (Dick) School of Veterinary Studies, Easter Bush Campus, Midlothian,
18 Scotland, EH25 9RG

19 ⁴ Marine Institute, Fish Health Unit, Rinville, Oranmore, Co. Galway, Ireland, H91 R673

20 ⁵ School of Veterinary Sciences, University of Bristol, England, BS40 5DU

21

22 **Acknowledgements**

23 The authors would like to thank Dr William Roy and Mr Chessor Matthews at the Machrihanish
24 Marine Environmental Research Laboratory (MERL) for their invaluable advice and help with
25 planning and conducting the AGD cohabitation challenge and sampling. The TEM imaging

26 was performed at the Electron Microscopy Lab., University of Edinburgh – with special thanks
27 to Mr Steven Mitchell for his excellent technical skill in sample preparation and assistance with
28 imaging. The authors would also like to thank Ms. Debbie Faichney for her technical advice
29 and support with histology. This study has received funding from the European Union’s
30 Horizon 2020 research and innovation programme under Grant Agreement no. 634429
31 (ParaFishControl). This output reflects only the author’s view and the European Union cannot
32 be held responsible for any use that may be made of the information contained herein.
33 Biotechnology and Biological Sciences Research Council grant award reference:
34 BB/M028224/1.

35

36 **Conflict of Interest**

37 No potential conflict of interest of all authors is reported.

38 **Abstract**

39 Amoebic gill disease (AGD) is emerging as one of the most significant health challenges
40 affecting farmed Atlantic salmon in the marine environment. It is caused by the amphizoic
41 amoeba *Neoparamoeba perurans*, with infestation of gills causing severe hyperplastic lesions,
42 compromising overall gill integrity and function. This study used histology, transmission
43 electron microscopy (TEM), immunohistochemistry and transcript expression to relate AGD-
44 associated pathological changes to changes in the morphology and distribution of chloride cells
45 (CCs) in the gills of Atlantic salmon (*Salmo salar* L.) showing the progression of an AGD
46 infection. A marked reduction in numbers of immunolabeled CCs were detected and a
47 changing pattern in distribution and morphology was closely linked with the level of basal
48 epithelial hyperplasia in the gill. In addition, acute degenerative ultrastructural changes to
49 CCs at the lesion site were observed with TEM. These findings were supported by the
50 early onset down-regulation of Na⁺/K⁺-ATPase transcript expression. This study provides
51 supportive evidence that histological AGD lesion assessment was a good qualitative tool
52 for AGD scoring and corresponded well with qPCR genomic *P. perurans* quantification.
53 Ultrastructural changes induced in salmon CCs as a result of AGD are reported here for
54 the first time.

55

56 **Keywords:** *Neoparamoeba perurans*, mitochondria rich cell, Na⁺/K⁺-ATPase, ionoregulatory
57 cells, salmonid, transmission electron microscopy.

58

59 **Introduction**

60 Amoebic gill disease (AGD) is one of the most significant health challenges affecting
61 farmed Atlantic salmon (*Salmo salar* L.) in the marine environment (Adams, Crosbie, &
62 Nowak, 2012) First reported in farmed salmon stocks in Tasmania in the mid 1980s
63 (Munday, 1986), it has since been found in most Atlantic salmon producing regions
64 worldwide *i.e.* France (Findlay & Munday, 1998), Ireland (Rodger & McArdle, 1996),
65 Spain (Rodger & McArdle, 1996), Chile (Bustos, Young, Rozas, Bohle, Ildefonse,
66 Morrison, & Nowak, 2011), Norway (Steinum, Kvellestad, Rønneberg, Nilsen, Asheim,
67 Fjell, Nygard, Olsen, & Dale, , 2008), Faroe Islands (Oldham, Rodger, & Nowak, 2016) and
68 South Africa (Mouton, Crosbie, Cadoret, & Nowak, 2014). Of further concern in Norway,
69 AGD has now been described in the cleaner fish species used to delouse farmed Atlantic
70 salmon infected with sea lice *Lepeophtheirus salmonis*, including Ballan wrasse *Labrus*
71 *bergylta* (Karlsbakk, Olsen, Einen, Mo, Fiksdal, Aase, Karkgraff, Skar, & Hansen, 2013) and
72 lumpfish *Cyclopterus lumpus* (Haugland, Olsen, Rønneseth, & Andersen, 2017). In Scotland,
73 AGD has been an emerging and serious problem since 2006 and is associated with major
74 economic losses due to a reduction in growth, increased mortality and related treatment
75 expenses (Rodger, 2014; Shinn, Pratoomyot, Bron, Paladini, Brooker, & Brooker, 2015). It
76 was estimated that AGD-related mortality losses cost around £10 million GBP in 2006 in
77 Norway and £60 million GBP in 2011 in Scotland (Shinn et al., 2015).

78

79 The aetiological agent of AGD is *Neoparamoeba perurans*, a cosmopolitan, free-living
80 marine amphizoic amoeba (Young, Crosbie, Adams, Nowak, & Morrison, 2007).

81 Amoebae attach to the gills causing white raised lesions, usually beginning at the base of
82 the filaments and spreading along the gill arch (Nowak, 2012). Infected gills often
83 covered with abundant mucus secretion when observed during routine gill examination

84 (Nowak & Munday, 1994; Rodger & McArdle, 1996; Taylor, Kube, Muller, & Elliott, 2009;
85 Nowak, 2012). The pathological sequence of AGD infection is well documented (Zilberg
86 & Munday 2000; Nowak & Munday 1994; Adams and Nowak 2001; Adams and Nowak
87 2003; Morrison, Cooper, Koop, Rise, Bridle, Adams, & Nowak, 2006; Young, Cooper,
88 Nowak, Koop, & Morrison, 2008) and has been characterised as ‘a focal fortification
89 strategy of the host tissue concurrent with a migration of immunoregulatory cells to
90 lesion-affected areas’ (Adams & Nowak, 2003). Other clinical signs include lethargy,
91 respiratory distress and an increased rate of opercular movement (Munday, Zilberg, &
92 Findlay, 2001). The severity and progression of the disease are routinely monitored and
93 scored according to the gill scoring system described by Taylor, Muller, Cook, Kube &
94 Elliott (2009) in which macroscopic pathology of the gills is described on a scale of clear
95 (0) to heavy (5).

96
97 Chloride cells (CCs) (also known as mitochondria-rich cells or ionocytes) are highly
98 specialised cells that are present on the afferent edge of the filamental epithelium of the
99 gill, in particular in the interlamellar region (Perry, 1997; Van Der Heijden, Van Der
100 Meij, Flik, & Wendelaar Bonga, 1999; Wilson & Laurent, 2002). Changes in the
101 distribution dynamics of chloride cells have been described during the progression of
102 AGD infections (Adams & Nowak, 2001; Adams & Nowak, 2003; Roubal, Lester &
103 Foster, 1989; Munday, Forster, Roubal, & Lester, 1990; Nowak & Munday, 1994).
104 Immunohistochemical identification of chloride cells, using anti- Na^+/K^+ -ATPase, shows
105 the sloughing of chloride cells from a forming lesion and fewer CCs found in association
106 with larger lesions (Adams & Nowak, 2001) with a concomitant reduction in Na^+/K^+ -
107 ATPase positive chloride cells in association with larger advanced stage lesions similarly

108 reported (Adams & Nowak, 2001; Adams & Nowak, 2003; Roubal, Lester & Foster,
109 1989; Munday, Forster, Roubal, & Lester, 1990; Nowak & Munday, 1994).

110

111

112 The aim of this study was to expand the current knowledge concerning the histopathological
113 and specifically ultrastructural characteristics of lesions associated with the early stage changes
114 occurring in an AGD infection and, in particular, its impact on the integrity and distribution of
115 gill chloride cells (CCs). The aims of the study were thus to (1) examine histological changes
116 of gills during the early stages of AGD infection (*i.e.* gill score of less than two) (2) measure
117 gill Na⁺/K⁺-ATPase transcript expression and (3) relate these findings to morphological,
118 ultrastructural and distributional changes of CCs as a response to early stage AGD in Atlantic
119 salmon. The study predominantly focused on evaluation of experimental data collected from
120 fish showing early signs of AGD infection (*i.e.* gill score of less than two), with comparative
121 analysis also conducted using archival histological materials from Atlantic salmon with high
122 gill score for infection with AGD (*i.e.* gill score of four and above).

123

124

125 **Materials and methods**

126 **Experimental fish**

127 All sampling in the present study was carried out at the Marine Environmental Research
128 Laboratory (MERL), Institute of Aquaculture, Machrihanish, Scotland, UK, 55.4 N 5.7
129 W).

130

131 A group of stock fish that had arrived from a freshwater facility to the current sea water
132 facilities in September 2015 were held in a 13000 L tank. The facility is supplied with flow-

133 through sea-water (35 ppt) filtered at 100 μm . All fish were maintained under ambient
134 temperature (min.: 11 $^{\circ}\text{C}$, max.: 13 $^{\circ}\text{C}$) and fed with commercial salmon pellets equivalent
135 to 1% of their body weight per day. These fish had been freshwater treated against AGD two
136 weeks prior to initiation of the experiment and had scored 0 for AGD afterwards, based on the
137 gill scoring system according to Taylor Muller, Cook, Kube, & Elliott, (2009).

138 Laboratory challenge of AGD was induced in Atlantic salmon using the cohabitation
139 method developed at the Institute of Aquaculture. Challenge cohabitants or ‘seeders’ were
140 produced using a stock of fish infected with AGD as part of an ongoing *in vivo* amoebae
141 challenge. Forty post-smolts were randomly selected from the above group of stock fish
142 and were cohabited in a 1-m-diameter tank (400 L) with 20 infected ‘seeder’ fish (mean
143 gill score of 1.5 ± 0.5), which had been previously ventrally panjet marked (Alcian blue, 0.065g
144 mL^{-1} , Sigma-Aldrich, UK) in order to allow their differentiation within the group. The level of
145 AGD infection within the challenged group was monitored weekly; fish were anaesthetised
146 using tricaine methanesulfonate (MS-222) at 75 mg/L and gross gill scores recorded, as
147 described above. Clinical signs of AGD were detected in challenged fish at 4 weeks post-
148 exposure *i.e.* gross gill score range; 0-1.5, based on the scoring system according to Taylor
149 Muller, Cook, Kube, & Elliott, (2009) and the sampling process was immediately initiated.
150 This was carried out in May 2016.

151 Fish husbandry, welfare and experimental protocols were conducted according to UK Home
152 Office requirements under the Animals (Scientific Procedures) Act 1986.

153

154 **Fish sampling**

155 A total of 15 fish were randomly sampled from amongst the challenged group; fish (weight
156 range 0.67 – 1.08 kg; fork length range 37.4 – 50 cm), euthanised by anaesthetic overdose
157 (MS-222) followed by destruction of the brain (Schedule 1 method: 4.2 of the Home Office

158 guidelines). In addition a further five fish were randomly sampled from amongst the stock
159 group of non-experimentally challenged fish (weight range 0.41 – 0.65 kg; fork length range
160 32.7 – 37.1 cm) as above. Gross gill scores were recorded from all sampled fish, as described
161 above and, based on these observed scores, four infection level categories (Clear (A), Very
162 Light (B), Light (C) Very Mild (D)) were designated to enable the different grades of early
163 stage AGD (*i.e.* gross gill score range; 0-1.5; Table 1) to be distinguished.

164

165 In addition, wax embedded gill tissues, obtained from a previous 4-week AGD cohabitation
166 challenge conducted in April 2014 at the same research facility, was used (Chalmers, Taylor,
167 Roy, Preston, Migaud, & Adams, 2017). Fish had been sampled at week 4 post-challenge when
168 fish were displaying gross gill scores of 3.5-4.5 and were grouped within the infection level
169 category; Heavy (E) (Table 1).

170

171 **Histology**

172 For histological analysis of samples taken in 2016, the entire third left gill arch was excised,
173 rinsed briefly in seawater and fixed in 10% neutral buffered formalin until processing and
174 embedding in paraffin wax. Gill samples from the previous challenge experiment in 2014 had
175 been taken from the second left gill arch, fixed in 4% paraformaldehyde for 24 h at 20 °C then
176 transferred to 70% ethanol prior to processing and embedding. All tissues were then sectioned
177 at 5 µm, stained with haematoxylin and eosin, screened microscopically using an Olympus
178 CX31 microscope (Olympus Life Science Solutions, Southend-on-Sea, UK) and then digitised
179 in high resolution for further analysis using an Axio Scan.Z1 slide scanner (ZEISS, Cambridge,
180 UK).

181

182 **Semi-quantitative lesion assessment**

183 From the histological examination, histological changes of gills were evaluated and grouped
184 into 3 categories: 1/ Small Focal, 2/ Medium Focal and 3/ Locally Extensive. Five filaments
185 showing visible signs of AGD infection were selected from three individual fish within each
186 infective category (Group A, B, C, D & E; Table 1). The total number of lesions visible
187 amongst the five filaments were counted and grouped into the respective lesion categories. A
188 filament was only counted when the central venous sinus was visible along two-thirds of the
189 filament length and secondary lamellae were the same length bilaterally till the tip of the
190 filament (Speare, Arsenault, MacNair, & Powell, 1997).

191

192 **Immunohistochemistry**

193 A portion of gill containing a visible lesion (consisting of 10-15 filaments) from the second left
194 gill arch was removed, rinsed in seawater and fixed in 4% paraformaldehyde for 24 h at 20 °C.
195 It was then transferred to 70% ethanol and stored at -20°C for immunohistochemical analysis
196 (IHC). A monoclonal antibody (MAb) against Na⁺/K⁺-ATPase (IgGα5), used to specifically
197 label chloride cells, was obtained from the Developmental Studies Hybridoma Bank,
198 Department of Biological Sciences, University of Iowa, Iowa, USA.

199

200 Samples were processed, embedded in paraffin wax and then sectioned. Sections were de-
201 waxed by placing the slides in successive xylene baths (2 x 5 min) and gradually rehydrated
202 through graded alcohol baths. The targeted tissues on the sections were encircled with wax by
203 using PAP pen (ImmEdgeTM pen, Vector Labs, California, UK) to keep reagents localised on
204 the tissue preparations. To inhibit endogenous peroxidase activity and block non-specific
205 binding sites, sections were incubated in 3% (v/v) hydrogen peroxide in methanol for 10 min
206 at 20°C, washed in the PBS (3 x 3 min) and then incubated with 10% normal goat serum for
207 30 min at 20°C. Primary antibody (anti-Na⁺/K⁺-ATPase; Mab, IgGα5), diluted 1:200, was

208 added for 1 h at 20°C and the sections were washed with PBS (3 x 3 min). The sections were
209 then incubated with goat anti-mouse IgG MAb conjugated to horseradish peroxidase (HRP)
210 (1:100, A4416, Sigma, USA) for 1 h at 20°C. Sections were then washed in tap water (3 x 10
211 min) and bound antibody peroxidase was labelled by using ImmPACT DAB Peroxidase (HRP)
212 Substrate (SK-4105; Vector Laboratories, USA) according to the manufacturer's instructions.
213 Sections were counterstained with Mayer's haematoxylin for 4 min, washed thoroughly with
214 tap water and gradually dehydrated (70% ethanol for 3 min, 100% ethanol for 5 min and 2
215 successive xylene baths (5 min each)), Slides were then coverslipped using Pertex™ before
216 being examined under an Olympus CX31 light microscope (Olympus Life Science Solutions,
217 Southend-on-Sea, UK), and digitised in high resolution for further analysis using an Axio
218 Scan.Z1 slide scanner (ZEISS, Cambridge, UK).

219

220 Negative control IgG isotype-matched MAbs were included in each IHC run and included
221 sections incubated with mouse monoclonal IgG Anti-Green fluorescent protein (GFP)
222 antibodies (1:500, Roche, Germany). Secondary antibody negative controls included sections
223 incubated in PBS instead of MAbs.

224

225 **Transmission electron microscopy (TEM)**

226 For ultrastructural examination, a 4-5 filament wide portion of gill from the second left gill
227 arch containing a visible lesion was taken from three fish from Group D (Infection level
228 category; very mild) and a similar sized portion of gill from the second left gill arch was taken
229 from three fish from Group A (Infection level category; clear). Samples were fixed in 3%
230 glutaraldehyde for 3 h, washed in PBS (3 x 10 min) and stored at 4°C. Samples were then
231 washed in 0.1 M sodium cacodylate buffer (3 x 10 min), post-fixed in 1% osmium tetroxide in
232 0.1 M sodium cacodylate (45 min) and finally washed in 0.1 M sodium cacodylate buffer (3 x

233 10 min). Samples were dehydrated in a series of graded ethanol (50, 70, 90 and 100%) in
234 propylene oxide (2 x 10 min) and embedded in TAAB 812 resin (TAAB Laboratories
235 Equipment, Berkshire, UK). Sections were cut at 60 nm and subsequently stained using uranyl
236 acetate and lead citrate for contrast then examined under JEOL JEM-1400 Plus transmission
237 electron microscope (JEOL, USA). Digital images were collected from a GATAN one view
238 camera (GATAN, USA).

239

240 **Molecular analyses**

241 For molecular analyses, small pieces of gill (4-5 filaments) were taken from sites with a visible
242 lesion (L) and no visible lesion (N) from the second left gill arch and immediately preserved
243 either in 1 mL 90% ethanol and stored at -20 °C or 1 mL RNAlater® (Thermo Fisher Scientific)
244 and stored at -70 °C for qPCR verification and quantification of *P. perurans* and down-stream
245 gene expression analysis of Na⁺/K⁺-ATPase, respectively. For Group A (clear) two pieces of
246 apparently uninfected tissue were taken randomly.

247 **Real time qPCR**

248 **DNA extraction**

249 Total DNA was extracted from gills (100 mg) which had been previously fixed in 90% ethanol.
250 DNA was extracted using the QiAamp tissue mini kit® (Qiagen) according to the
251 manufacturer's protocol for purification from animal tissues. The quality and quantity of
252 extracted DNA was checked and measured by NanoDrop (Nanodrop 1000, Thermo Fisher
253 Scientific, UK) and all DNA samples were standardised to the concentration of 50 nMol μL⁻¹
254 and stored at -20 °C.

255

256 **Genomic qPCR for *P. perurans* detection and quantitation**

257 The extracted DNA samples were used for quantification and confirmation of the presence of

258 *P. perurans* by real-time qPCR at the Marine Institute in Galway, Ireland according to Downes,
259 Henshilwood, Collins, Ryan, O'Connor, Rodger, MacCarthy & Ruane (2015). The *N. perurans*
260 loading obtained from Groups A-E were statistically compared using non-parametric Kruskal-
261 Wallis test following an Anderson-Darling test for normality using Minitab® 17 software
262 (Minitab Ltd, Coventry, UK)). For *post-hoc* testing, the Mann-Whitney U test (Minitab® 17
263 software (Minitab Ltd, Coventry, UK)) was used.

264

265 **RNA Extraction**

266 Total RNA was extracted from gills (approximately 100 mg) that had previously been stored
267 in RNAlater, using the TRIzol® extraction technique (Thermo Scientific, UK) according to
268 manufacturer's instructions with modifications. Briefly, the samples were incubated with
269 TRIzol® on ice for 30 min before homogenising with 5 metal beads (BioSpec Products, UK)
270 using a Mini-Beadbeater (Mini-Beadbeater-16, BioSpec Products, USA) for 60 sec. Following
271 organic solvent extraction with TRIzol, RNA was precipitated in 200 µL RNA precipitation
272 solution (1.2M NaCl, 0.8 M Sodium Citrate Sesquihydrate (Sigma Aldrich, UK)) combined
273 with 200 µL isopropanol (Sigma Aldrich, USA) then incubated at 20 °C for 10 min prior to
274 centrifugation at 20,000 x *g* for 10 min at 4 °C. The RNA pellet was washed in 1 mL of 75 %
275 ethanol and left to air dry for 5 min at 20 °C. RNA was then dissolved in 50 µL of RNase free
276 water (Thermo Scientific, UK) on ice before measuring RNA quality and quantity by
277 NanoDrop (Nanodrop 1000, Thermo Scientific). RNA samples were diluted to a concentration
278 range of 300 and 600 ng µL⁻¹ before storing at -70 °C until RT-qPCR analysis was performed
279 at Harper Adams University, UK.

280

281 **Complementary DNA (cDNA) synthesis**

282 First strand cDNA synthesis for 1 µg of extracted total RNA for the RT-qPCR was carried out

283 using a High Capacity cDNA Reverse Transcription Kit (Applied BioSystems, UK) according
284 to the manufacturer's instructions. The master mix with reverse transcriptase was prepared for
285 all samples ($n = 38$) adding 2 μL of x10 RT buffer, 0.8 μL dNTP mix (100 mM each), 2 μL
286 10x RT random primers and 1 μL reverse transcriptase (50 U μL^{-1}) and 4.2 μL nuclease free
287 water. In parallel, two randomly selected samples were prepared using the same master mix
288 but free of reverse transcriptase as an RT- (negative control) to determine genomic
289 contamination. The reverse transcription reaction was then performed by adding samples to a
290 thermocycler (Biometra R) and incubating at 25 °C for 10 min, 37 °C for 2 h and finally 85 °C
291 for 5 min to inactivate the DNA polymerase. The cDNA samples were placed directly on ice
292 for immediate PCR or frozen at -20 °C for later analysis.

293

294 **Real time qPCR**

295 Primer sequences for the target gene (Na^+/K^+ -ATPase) and the reference genes (β -Actin, ELF-
296 1 and Cofilin-2) genes were obtained from Eurofins MWG synthesis GmbH (Ebersberg,
297 Germany) and tested for primer efficiency and quality by generating a standard curve using a
298 pooled cDNA sample prepared from mixing 3 μL of stock cDNA, prior to use in RT-qPCR
299 assay (Table 2) and carrying out melting curve analysis.

300

301 The real-time qPCR assay was performed in compliance with MIQE guidelines (Bustin, Benes,
302 Garson, Hellemans, Huggett, Kubista, Mueller, Nolan, Pfaffl, Shipley, Vandesompele, &
303 Wittwer, 2009). The cDNA samples and RT- sample were diluted 1:20 using RNase free
304 water. For each gene, RT-qPCR assay based on SYBR green chemistry was performed in a
305 Bio-RAD, T100™ qPCR machine using white 96-well plates. The RT-qPCR master mix for
306 samples, standard curve (*i.e.* serial dilution of cDNA pool), non-template control (NTC) and
307 internal control (IC) were prepared by mixing 10 μL of Luminaris Color HiGreen qPCR Master

308 Mix (Fisher Scientific, UK), 1 μL each of Forward Primer and Reverse primer (10 pmol μL^{-1})
309 and 3 μL of water.

310

311 The templates (5 μL) and master mix (15 μL) were loaded into the PCR plate (final volume of
312 20 μL per sample), before the plate was vortexed (Camlab, UK) and centrifuged by using c1000
313 Mini Plate Spinner centrifuge. The assay was thermocycled at; UDG pre-treatment at 50 $^{\circ}\text{C}$ (2
314 min), an initial denaturation of 95 $^{\circ}\text{C}$ for 10 min, followed by 40 cycles of 95 $^{\circ}\text{C}$ (15 sec),
315 annealing temperature 58 $^{\circ}\text{C}$ (30 sec) and extension 72 $^{\circ}\text{C}$ (30 sec), according to the
316 manufacturer's protocol. The melting curve (dissociation peak) analysis was performed at 70
317 – 90 $^{\circ}\text{C}$ measuring every 0.5 $^{\circ}\text{C}$ to evaluate primer dimer and genomic contamination.

318

319 **Gene Expression Analysis**

320 The mean Ct values calculated within the Bio-Rad software were exported to Excel. The gene
321 expression analysis was subsequently carried out using GenEx Enterprise software (version
322 5.4.3). The expression values (Ct) of the Na^+/K^+ -ATPase were normalised against three
323 reference genes (ELF-1, β -Actin and Cofilin-2, reference gene index). The relative expression
324 value of the test group compared to control (*i.e.* non-AGD challenged) fish was estimated
325 before testing statistical differences between test groups using Minitab[®] 17 software (Minitab
326 Ltd, Coventry, UK). The normalised mean gene expression values were compared against the
327 control group for any statistical differences using a parametric General Linear Model (GLM)
328 and *post-hoc* test with Bonferroni correction.

329

330 **Results**

331 **Gill histology**

332 Histological examination of samples indicated the presence of AGD-associated focal lesions
333 affecting the secondary lamellae from gills of fish from Groups B-E (n = 5) (Fig. 1).

334

335 The histologically observed AGD lesions were graded into 3 different categories, based on
336 their microscopic pathology *i.e.* (A) small focal, (B) medium focal and (C) locally extensive.

337 These were characterised as follows:

338

339 1) Small Focal; focal lesions characterised by two different types of pathological findings: 1)
340 Basal hyperplasia; normally involving 2-3 secondary lamellae and variable levels of basal
341 epithelial hyperplasia in the interlamellar space affecting <50 % of the length of the secondary
342 lamellae (Fig. 1A&B). The epithelial cells in the affected areas were marked by hyperplasia
343 and oedema (Fig. 1A&B). 2) Distal lamellar hypertrophy; consisting of lamellar swelling and
344 fusion observed at the distal ends of 2-3 secondary lamellae causing the formation of
345 interlamellar lacunae. Such lesions were associated with a varying degree of hyperplasia and
346 intercellular lamellar oedema (Fig. 1A&C).

347

348 2) Medium Focal; lesions were defined as segmental lesions affecting between 4-15 secondary
349 lamellae. These lesions were characterised by the presence of marked basal epithelial
350 hyperplasia involving >50 % of the length of the secondary lamellae causing fusion of several
351 lamellae together forming a segment (Fig. 1D). These hyperplastic basal epithelial cells showed
352 hydropic degenerative changes with interstitial and intercellular oedema detected within
353 lesions. Hydropic degeneration of epithelial cells was more marked at the distal end of the
354 secondary lamellae extending proximally to the base, often giving a disruptive look to the
355 epithelial surface of the lesion (Fig. 1D).

356

357 3) Locally extensive; lesions affecting more than 15 secondary lamellae displayed a complete
358 loss of normal lamellar architecture (Fig. 1E). The affected region included >50 % of the length
359 of the secondary lamellae. The cells were spongiotic and showed both hypertrophic and
360 hyperplastic responses with large areas of degenerated cells and intercellular oedema (Fig. 1E).
361 The marked lamellar hyperplasia resulted in lamellar fusion along the filament which
362 contributed to the 'clubbing' appearance of filaments (not shown). An abundance of mucous
363 cells was detected on the surface of the lesions in close contact with the amoebae (*N. perurans*)
364 (Fig. 1E). Amoebae were often present in surface mucus and were particularly abundant at the
365 site of sloughing surface epithelial cells (Fig. 1E). Figure 1F shows histologically normal gills
366 from a Group A fish.

367

368 **Semi-quantitative lesion assessment**

369 Based on the semi-quantitative assessment, the number and severity of the focal lesions was
370 seen to be associated with an increase in gross gill score (Fig. 2). As gross gill score increased,
371 there was a shift in the number of observed lesions from small focal to medium focal. Whilst
372 the proportion of lesions was similar in two different groups (Groups B and C), a higher
373 proportion of medium focal lesions was detected in the fish with higher AGD scores (Group
374 D). Within the heavy infection level category (Group E), the overall number of lesions was
375 reduced due to the enlarged surface areas of both medium focal and locally extensive lesions.

376

377 **Immunohistochemistry**

378 Examination of immunolabeled slides indicated a high specificity of the mouse monoclonal
379 antibody against Na⁺/K⁺-ATPase for chloride cells in the gills of Atlantic salmon. No cross
380 reactivity was detected from the isotype control or the PBS control.

381

382 Based on the observed immunolabeling, chloride cells in non-affected areas of gills were found
383 abundantly distributed at the interlamellar regions and junctions between the filament and
384 lamellae (Fig. 3A). Rarely, chloride cells were found distributed along the lamellae (Fig. 3A).
385 Within the category of lesions classified as ‘small focal’ (Fig 3B-F), there was a marked
386 reduction in chloride cells in the interlamellar regions, with concurrent mild basal hyperplasia
387 of the epithelium. Multiple oedematous spaces were noted at the sites where chloride cells were
388 previously located (Fig. 3B, C & F). With increasing lesion size, the level of basal hyperplasia
389 was more marked and the hyperplastic region extended across to the interlamellar region of the
390 neighbouring lamellae (Fig. 3E). In these ‘small focal’ lesions, the number of chloride cells
391 was only markedly reduced at the centre of the lesion (the initial lesion) with intact chloride
392 cells within the neighbouring lamellar region (Fig. 3B, C). These intact chloride cells were
393 lifted distally by the proliferative basal epithelial lining (Fig. 3D). As hyperplasia progressed,
394 sloughing of chloride cells was observed within the lamellar space (Fig. 3E). As the chloride
395 cells moved along the lamellae, signs of hydropic degenerative changes were evident and
396 ultimately replaced by formation of oedematous spaces close to the lesion surface (Fig. 3F).

397

398 Depending on the extent of basal proliferation of each interlamellar region, the chloride cells
399 appear only at the border of lesions (Fig. 4A). Throughout the progression of the lesion,
400 minimal regeneration of the chloride cells was observed as no increase in the number of
401 immunolabeled cells was evident. When a distal lamellar hypertrophic lesion was observed, no
402 initial reduction in chloride cells was found in the interlamellar region or filament-lamellar
403 junction (Fig. 4B). When “medium focal” and “locally extensive” lesions were examined, the
404 lesions ranged from minimal immunolabeling at the lesion border to a complete absence of
405 chloride cells within the lesion (Fig. 4C-D).

406

407 **Transmission Electron Microscopy**

408 Transmission electron microscopy was employed to examine the ultrastructural changes of
409 chloride cells in association with AGD infection by using fish samples from Group A (Infection
410 level category; clear) and Group D (Infection level category; very mild).

411 Normally appearing chloride cells from the uninfected gill tissues were characterised by their
412 columnar shape, high numbers of electron dense mitochondria and a well-developed vesicular
413 tubular network in close association with the endoplasmic reticulum in the cytoplasm (Fig. 5A,
414 B). At the apical portion of the cell, vesicles and short tubules replace the more extensive
415 intricate vesicular tubular network of the basolateral portion (Fig. 5C). Mitochondria were
416 characterised by a well demarcated double enveloped membrane with well-defined infoldings
417 of cristae closely linked to the inner membrane of the mitochondria (Fig. 5D).

418

419 The surface of the gill lamellae in fish from Group D appeared oedematous with multiple areas
420 of epithelial hyperplasia. In some areas, there was separation of epithelial lining from the
421 basement membrane due to intercellular oedema (Fig. 6A). Hydropic degeneration was evident
422 in multiple chloride cells on the lamellar surface, recognised by cell swelling, electron lucent
423 cytoplasm due to the formation of multiple vacuoles and marked loss of endoplasmic tubular
424 details (Fig. 6B). On the apical membrane, there was the fusion and loss of microridges (Fig.
425 6C). The swollen mitochondria were characterised by an ill-defined envelope, an electron
426 lucent matrix and distorted cristae. (Fig. 6D).

427 **Real-time-qPCR of *P. perurans* quantification and Na⁺/K⁺-ATPase gene expression**

428 The real-time qPCR results for *P. perurans* quantification and Na⁺/K⁺-ATPase relative
429 expression assays are shown in Figs. 7 and 8 respectively. An increase in *P. perurans* load
430 is seen to correlate with an increase in gross gill scores (Fig. 7). However the Group A
431 (clear) fish, who displayed no macroscopic gross gill scores to suggest AGD infection,

432 exhibited a low level of genomic *N. perurans* DNA equivalents (Fig. 7A). The likely reason
433 for this is the non-experimentally challenged fish, from which Group A were selected, had
434 come into previous contact with *N. perurans* through the inlet water supply pumped
435 directly from the sea at the research facility. Fish had been treated with freshwater two
436 weeks prior to this experiment.

437

438 The relative expression level of Na⁺/K⁺-ATPase transcript (Fig. 8) was notably down-regulated
439 in AGD-challenged fish compared to fish from the non-experimentally challenged group
440 (Group A), with the exception of Group B (Very Light; AGD score: 0-0.5; *n* = 5) (L; tissues
441 from lesion site) (Fig. 7B).

442

443 Interestingly both the amoebic load (Fig. 7) and the level of Na⁺/K⁺-ATPase (Fig. 8) gene
444 expression in tissues from lesion site (L) and apparently normal tissues from adjacent to
445 lesion site (N) were not found to be statistically different.

446

447 **Discussion**

448 There have been limited studies to date focusing on the implications of early stage AGD
449 in Atlantic salmon. Considering the variable efficacy of hydrogen peroxide treatment
450 (Adams, Crosbie, & Nowak, 2012; Powell & Clark, 2003) the logistic and economic
451 problems associated with freshwater treatment (Nowak, 2012) and the difficulty of
452 controlling the disease at higher temperatures, early detection and prevention are critical
453 for AGD management in commercial Atlantic salmon aquaculture. Therefore, a better
454 understanding of early stage AGD-associated gill lesions is crucial to the timely
455 management of the disease.

456

457 The histopathological findings from the present work resembled common findings in
458 previously published AGD studies *i.e.* variable levels of basal epithelial hyperplasia and
459 subsequent lamellar fusion, which became increasingly extensive as the lesion advances
460 (Munday, Foster, Roubal & Lester 1990; Nowak & Munday 1994; Adams & Nowak 2001;
461 Adams, Ellard & Nowak 2004). Ultrastructural examination of gill epithelium and chloride
462 cells in AGD infected gills using TEM revealed signs of oedema and epithelial
463 hyperplasia, even in fish scored as having very mild AGD lesions (Group D). The observed
464 hydropic degeneration and loss of apical microridges in CCs strongly suggest the
465 likelihood of severe functional impairment, even where CCs are still visible by light
466 microscopy, and could have implications for ion and pH regulation in these fish and thus
467 for wider health and welfare indicators (Van Der Heijden et al., 1999).

468

469 In the present study, histological assessment of AGD-related lesions corresponded well to
470 the qPCR *P. perurans* quantification; for example, the increased levels of *P. perurans* in
471 Group D (very mild; gross gill score: 1.0-1.5) and Group E (heavy; gross gill score 3.5-
472 4.5) compared to Group A (clear; gross gill score 0) was supported by the increased
473 number of medium focal and locally extensive lesions within these groups when compared
474 to Group A. However, a disparity has previously been reported between diagnostic
475 methods used for AGD; Atlantic salmon gills displaying grossly visible lesions did not
476 show the presence of *P. perurans* at a histological level, with this discrepancy deemed
477 likely to be due to the sampling technique during gill excision *i.e.* only one section from
478 one gill arch was examined for subsequent histological analysis (Clark & Nowak, 1999)
479 and also loss of mucus and associated amoebae during fixation. It is indeed well
480 established that conventional fixatives often wash away the overlaying mucus layers (Lee
481 Schurch, Roth, Jiang, Cheng, Bjarnason & Green, 1995; Mays, Feldhoff, & Nettleton, 1984)

482 and associated amoebae, hence the need for alternative methods to optimise fixation to
483 enable mucus stabilisation and allow a better understanding of parasite interactions with
484 gill mucus during AGD infection (Fernandez, Mascolo, Monaghan, Baily, Chalmers,
485 Paladini, Adams, Bron, & Fridman, 2019). In the current study, gills for subsequent
486 downstream molecular analysis of *P. perurans* load was taken from a section of gill
487 displaying grossly visible AGD lesions which would most likely account for the correlation
488 seen.

489

490 The identification of *P. perurans* by molecular analysis in fish from Group A (no
491 macroscopic signs of infection) is in agreement with previous studies where grossly visible
492 white patches, used for presumptive diagnosis were not found in AGD infected rainbow
493 trout (*Onchorhynchus mykiss*) (Munday, Foster, Roubal, & Lester, 1990) and Atlantic
494 salmon (Clark & Nowak, 1999) suggesting this method is only reliable in cases of heavy
495 AGD infection. When appraising the findings of this study, it is vital to evaluate the
496 experimental limitations. As the results indicated, the control fish (Group A) were not free
497 from AGD as both *P. perurans* loads and histological AGD lesions were detected from the
498 samples. This was due to the presence of *P. perurans* in the inlet water resulting in a
499 naturally occurring infection. At present, there is a shortage of commercial AGD- specific
500 pathogen free fish. Many current studies are being carried out to explore the possibility of
501 selective breeding for AGD resistance as there is evidence of heritable genetic variation in
502 AGD susceptibility in both survival and gross gill pathology (Taylor, Kube, Muller, & Elliott,
503 2009). In addition, in the current study, non-specific chronic gill changes were present on
504 occasion amongst fish within different AGD score groups which were characterised by the
505 presence of remodeling and healing fractures of gill cartilage surrounded by fibrotic capsules
506 of collagen and hyperplastic epithelial tissues indicating the chronic nature of these

507 pathologies. It was difficult to ascertain the causative agent for these types of lesions
508 however fish from the present study had previously been infected with AGD and
509 underwent freshwater treatment prior to the commencement of this cohabitation trial. It is
510 most likely that this cartilage remodelling represents chronic changes associated with
511 previously severe AGD infection.

512

513 Immunohistochemistry was used to examine distributional changes of chloride cells in
514 relation to AGD lesion development in the current study. The decrease in chloride cell
515 numbers was closely associated with the degree of basal epithelial hyperplasia. There was
516 an initial focal loss of chloride cells (from 1-2 inter-lamellar spaces) where minimal basal
517 epithelial hyperplastic changes were observed, suggesting the possible presence of
518 localised irritants such as the attachment of *P. perurans*. Previous studies have noted that
519 the subsequent development and progression of the lesion relies on the host's proliferative
520 response and migration of amoebae along the filament (Taylor, Muller, Cook, Kube, &
521 Elliott, 2009). As the level of basal epithelial hyperplasia increased at the centre of the
522 lesions, hydropic degeneration of the chloride cells was observed, which ultimately led to
523 formation of regional oedema and sloughing of degenerated chloride cells on the surface
524 of the lesions. The subsequent presence of chloride cells towards the distal end of the
525 lamellae was in accordance with previous reports in Atlantic salmon (Chalmers et al.,
526 2017).

527

528 It has been previously reported that no overall reduction in chloride cells was evident from
529 'mild' and 'moderate' infected fish by quantitative digital image analysis from a re-
530 infection AGD field trial (Adams & Nowak, 2003). This was most likely due to the
531 localised nature of the lesions which appeared in small numbers on the gill and thus had

532 very limited effect on the overall chloride cell numbers of the gills. In the current study,
533 by the time AGD lesions advanced to ‘medium focal’ or ‘locally extensive’ lesions, the
534 chloride cells were almost completely absent from these hyperplastic areas. The reduction
535 in chloride cells in the hyperplastic AGD lesions observed in the current study is supported
536 by previous studies (Adams & Nowak, 2003; Munday et al., 1990; Nowak & Munday,
537 1994; Roubal, Lester, & Foster, 1989).

538

539 Chloride cells are characterised by a columnar/ovoid appearance, sharing the same
540 ultrastructural features as other ion transport cells *e.g.* high mitochondrial density and a
541 well-developed vesicular-tubular network, which is continuous with the extensively
542 invaginated basolateral membrane (Van Der Heijden, Van Der Meij, Flik, & Wendelaar
543 Bonga, 1999). The extensive vesicular-tubular network within the cytoplasm provides a
544 large surface area for the ion-transport protein, Na⁺/K⁺-ATPase (Perry, 1997). Chloride
545 cells are believed to be the primary extra-renal site for regulation of osmotically active ion
546 concentrations, ultimately helping to regulate blood pH by manipulating the rates of Cl⁻
547 and Na⁺ ionic uptake, the activity of which mediates transfer of H⁺ and HCO₃⁻ (Evans,
548 Piermarini, & Choe, 2005; Laurent & Dunel, 1980). Apoptosis of CCs in teleosts has been
549 previously described under both pathogenic conditions *i.e.* toxicants in the rainbow trout (*O.*
550 *mykiss*) (Daoust, Wobeser, & Newstead, 1984; Mallat, 1985) and under physiological
551 conditions in newly hatched rainbow trout (Rojo, & Gonzalez, 1999), newly hatched brown
552 trout (*S. trutta*) (Rojo, Blanquez, & Gonzalez, 1997), the adult Mozambique tilapia (*O.*
553 *mossambicus*) (Wendelaar Bonga & van der Meij, 1989; Wendelaar Bonga, Flik, Balm, & van
554 der Meij, 1990) and the hybrid *O. mossambicus* x *Oreochromis urolepis hornorum* (Sardella,
555 Maey, Cooper, Gonzalez, & Brauner, 2004). These authors all report the ultrastructural
556 changes of MRCs as showing nuclear and cytoplasmic condensation and enlargement of the

557 mitochondria surrounded by a distended tubular system and oedematous areas, as reported in
558 the current study. In addition intracellular oedema caused a lifting of the epithelial lining and
559 loss of microridges was apparent.

560 To conclude, this study has added to pre-existing knowledge of host-pathogen interactions
561 underlying the early stages of AGD infection in Atlantic salmon and identified
562 distributional and morphological changes of chloride cells associated with them. A marked
563 reduction in chloride cells (*i.e.* Na⁺/K⁺-ATPase immunolabeling) was detected at the
564 interlamellar region of the gills and found to be closely linked to increasing levels of basal
565 epithelial hyperplasia from focal AGD lesions. Acute degenerative changes in chloride
566 cells at the lesion site were recognised by the use of TEM indicating cytoplasmic
567 condensation, and oedematous areas and microridge changes. Both distributional and
568 morphological changes were supported by the early onset down-regulation of Na⁺/K⁺-
569 ATPase gene expression. This work provides useful information about the effects of host-
570 pathogen interaction during AGD infection at a cellular level and their pathophysiological
571 implications.

572

573 **References**

574 Adams, M. B., Crosbie, P. B. B., & Nowak, B. F. (2012). Preliminary success using
575 hydrogen peroxide to treat Atlantic salmon, *Salmo salar* L., affected with
576 experimentally induced amoebic gill disease (AGD). *Journal of Fish Diseases*, 35(11),
577 839–848. <http://doi.org/10.1111/j.1365-2761.2012.01422.x>

578 Adams, M. B., Ellard, K., & Nowak, B. F. (2004). Gross pathology and its relationship with
579 histopathology of amoebic gill disease (AGD) in farmed Atlantic salmon, *Salmo salar*
580 L. *Journal of Fish Diseases*, 27, 151–161.

581 Adams, M. B., & Nowak, B. F. (2001). Distribution and structure of lesions in the gills of

582 Atlantic salmon, *Salmo salar* L., affected with amoebic gill disease. *Journal of Fish*
583 *Diseases*, 24(9), 535–542. <http://doi.org/10.1046/j.1365-2761.2001.00330.x>

584 Adams, M. B., & Nowak, B. F. (2003). Amoebic gill disease: sequential pathology in
585 cultured Atlantic salmon, *Salmo salar* L. *Journal of Fish Diseases*, 26, 601–614.
586 Retrieved from <http://doi.wiley.com/10.1111/j.1365-2761.2004.00531.x>

587 Bustin, S. A., Benes, V., Garson, J. A., Hellemans, J., Huggett, J., Kubista, M., ... Wittwer,
588 C. T. (2009). The MIQE guidelines: Minimum information for publication of
589 quantitative real-time PCR experiments. *Clinical Chemistry*, 55(4), 611–622.
590 <http://doi.org/10.1373/clinchem.2008.112797>

591 Bustos, P. A., Young, N. D., Rozas, M. A., Bohle, H. M., Ildefonso, R. S., Morrison, R. N.,
592 & Nowak, B. F. (2011). Amoebic gill disease (AGD) in Atlantic salmon (*Salmo salar*)
593 farmed in Chile. *Aquaculture*, 310, 281–288.
594 <http://doi.org/10.1016/j.aquaculture.2010.11.001>

595 Chalmers, L., Taylor, J. F., Roy, W., Preston, A. C., Migaud, H., & Adams, A. (2017). A
596 comparison of disease susceptibility and innate immune response between diploid and
597 triploid Atlantic salmon (*Salmo salar*) siblings following experimental infection with
598 *Neoparamoeba perurans*, causative agent of amoebic gill disease. *Parasitology*, 144(09),
599 1229–1242. <http://doi.org/10.1017/S0031182017000622>

600 Clark, A., & Nowak, B. F. (1999). Field investigations of amoebic gill disease in Atlantic
601 salmon, *Salmo salar* L., in Tasmania. *Journal of Fish Diseases*, 22(6), 433–443.
602 <http://doi.org/10.1046/j.1365-2761.1999.00175.x>

603 Daoust, P. Y., Wobeser, G., & Newstead, J. D. (1984). Acute pathological effects of
604 inorganic mercury and copper in gills of rainbow trout. *Veterinary Pathology*, 21, 93–
605 101.

606 Downes, J., Henshilwood, K., Collins, E., Ryan, A., O'Connor, I., Rodger, H., ... Ruane, N.

607 (2015). A longitudinal study of amoebic gill disease on a marine Atlantic salmon farm
608 utilising a real-time PCR assay for the detection of *Neoparamoeba perurans*.
609 *Aquaculture Environment Interactions*, 7(3), 239–251. <http://doi.org/10.3354/aei00150>

610 Evans, D. H., Piermarini, P. M., & Choe, K. P. (2005). The multifunctional fish gill:
611 dominant site of gas exchange, osmoregulation, acid-base regulation, and excretion of
612 nitrogenous waste. *Physiological Reviews*, 85, 97–177.
613 <http://doi.org/10.1152/physrev.00050.2003>.

614 Fernandez, C., Mascolo, D., Monaghan, S. J., Baily, J. L., Chalmers, L., Paladini, G., ...
615 Fridman, S. (2019). Methacarn preserves mucus integrity and improves visualization of
616 amoebae in gills of Atlantic salmon (*Salmo salar* L.). *Journal of Fish Diseases*, (April),
617 jfd.12988. <http://doi.org/10.1111/jfd.12988>

618 Findlay, V. L., & Munday, B. L. (1998). Further studies on acquired resistance to amoebic
619 gill disease (AGD) in Atlantic salmon, *Salmo salar* L. *Journal of Fish Diseases*, 21(2),
620 121–125. <http://doi.org/10.1046/j.1365-2761.1998.00086.x>

621 Haugland, G. T., Olsen, A. B., Rønneseth, A., & Andersen, L. (2017). Lumpfish (*Cyclopterus*
622 *lumpus* L.) develop amoebic gill disease (AGD) after experimental challenge with
623 *Paramoeba perurans* and can transfer amoebae to Atlantic salmon (*Salmo salar* L.).
624 *Aquaculture*, 478, 48–55. <http://doi.org/10.1016/j.aquaculture.2016.04.001>

625 Herath, T. K., Bron, J. E., Thompson, K. D., Taggart, J. B., Adams, A., Ireland, J. H., &
626 Richards, R. H. (2012). Transcriptomic analysis of the host response to early stage
627 salmonid alphavirus (SAV-1) infection in Atlantic salmon *Salmo salar* L. *Fish and*
628 *Shellfish Immunology*, 32(5), 796–807. <http://doi.org/10.1016/j.fsi.2012.02.001>

629 Karlsbakk, E., Olsen, A. B., Einen, A.-C. B., Mo, T. A., Fiksdal, I. U., Aase, H., ... Hansen,
630 H. (2013). Amoebic gill disease due to *Paramoeba perurans* in ballan wrasse (*Labrus*
631 *bergylta*). *Aquaculture*, 412–413, 41–44.

632 <http://doi.org/10.1016/j.aquaculture.2013.07.007>

633 Laurent, P., & Dunel, S. (1980). Morphology of gill epithelia in fish. *American Journal of*
634 *Physiology-Regulatory, Integrative and Comparative Physiology*, 238(3), R147–R159.
635 <http://doi.org/10.1152/ajpregu.1980.238.3.R147>

636 Lee, M. M., Schurch, S., Roth, S. H., Jiang, X., Cheng, S., Bjarnason, S., & Green, F. H. Y.
637 (1995). Effects of acid aerosol exposure on the surface properties of airway mucus.
638 *Experimental Lung Research*, 21(6), 835–851.
639 <http://doi.org/10.3109/01902149509031766>

640 Madsen, S. S., Kiilerich, P., & Tipsmark, C. K. (2009). Multiplicity of expression of
641 Na⁺,K⁺-ATPase alpha-subunit isoforms in the gill of Atlantic salmon (*Salmo salar*):
642 cellular localisation and absolute quantification in response to salinity change. *Journal*
643 *of Experimental Biology*, 212, 78–88. <http://doi.org/10.1242/jeb.024612>

644 Mallat, J. (1985). Fish gill structural changes induced by toxicants and other irritants: a
645 statistical review. *Canadian Journal of Fish and Aquatic Sciences*, 42, 630–648.

646 Mays, E. T., Feldhoff, R. C., & Nettleton, G. S. (1984). Determination of protein loss during
647 aqueous and phase partition fixation using formalin and glutaraldehyde. *Journal of*
648 *Histochemistry and Cytochemistry*, 32(10), 1107–1112.
649 <http://doi.org/10.1177/32.10.6434629>

650 Morais, S., Monroig, O., Zheng, X., Leaver, M. J., & Tocher, D. R. (2009). Highly
651 unsaturated fatty acid synthesis in Atlantic salmon: Characterization of ELOVL5- and
652 ELOVL2-like elongases. *Marine Biotechnology*, 11(5), 627–639.
653 <http://doi.org/10.1007/s10126-009-9179-0>

654 Mouton, A., Crosbie, P., Cadoret, K., & Nowak, B. (2014). First record of amoebic gill
655 disease caused by *Neoparamoeba perurans* in South Africa. *Journal of Fish Diseases*,
656 37(4), 407–409. <http://doi.org/10.1111/jfd.12133>

657 Munday, B. L. (1986). Diseases in salmonids. In J. D. Humphrey & J. S. Landon (Eds.),
658 *Diseases of Australian Fish and Shellfish* (pp. 127–141). Victoria: Department of
659 Agriculture and Rural Affairs.

660 Munday, B. L., Foster, C. K., Roubal, F. R., & Lester, R. J. G. (1990). Paramoebic gill
661 infection and associated pathology of Atlantic salmon, *Salmo salar* and rainbow trout,
662 *Salmo gairdneri* in Tasmania. In F. O. Perkins & T. C. Cheng (Eds.), *Pathology in*
663 *Marine Science* (pp. 215–222). San Diego: Academic Press.
664 <http://doi.org/10.1016/B978-0-12-550755-4.50026-4>

665 Munday, B. L., Zilberg, D., & Findlay, V. (2001). Gill disease of marine fish caused by
666 infection with *Neoparamoeba pemaquidensis*. *Journal of Fish Diseases*, 24(9), 497–507.
667 <http://doi.org/10.1046/j.1365-2761.2001.00329.x>

668 Nowak, B. F. (2012). *Neoparamoeba perurans*. In P. T. K. Woo & K. Buchmann (Eds.), *Fish*
669 *parasites: pathobiology and protection* (1st ed.). London: CABI International.

670 Nowak, B. F., & Munday, B. L. (1994). Histology of gills of Atlantic salmon during the first
671 few month following transfer to sea water. *Bulletin of the European Association of Fish*
672 *Pathologists*, 14(3), 77–81.

673 Oldham, T., Rodger, H., & Nowak, B. F. (2016). Incidence and distribution of amoebic gill
674 disease (AGD) - An epidemiological review. *Aquaculture*, 457, 35–42.
675 <http://doi.org/10.1016/j.aquaculture.2016.02.013>

676 Perry, S. F. (1997). The chloride cell: Structure and function in the gills of freshwater fishes.
677 *Annual Review of Physiology*, 59(9), 325–347.
678 <http://doi.org/10.1146/annurev.physiol.59.1.325>

679 Powell, M. D., & Clark, G. A. (2003). In vitro survival and the effect of water chemistry and
680 oxidative chemical treatments on isolated gill amoebae from AGD-affected Atlantic
681 salmon. *Aquaculture*, 220(1–4), 135–144. [http://doi.org/10.1016/S00448486\(02\)006294](http://doi.org/10.1016/S00448486(02)006294)

682 Rodger, H. D. (2014). Amoebic gill disease (AGD) in farmed salmon (*Salmo salar*) in
683 Europe. *Fish Veterinary Journal*, 14, 16–27.

684 Rodger, H. D., & McArdle, J. F. (1996). An outbreak of amoebic gill disease in Ireland.
685 *Veterinary Record*, 139(14), 348–349. <http://doi.org/10.1136/vr.139.14.348>

686 Rojo, C., & González, E. (1999). Ontogeny and apoptosis of chloride cells in the gill
687 epithelium of newly hatched rainbow trout. *Acta Zoologica*, 80, 11–23.

688 Rojo, M.C., Blanquez, M.J., & Gonzalez, M.E. (1997). Ultrastructural evidence for apoptosis
689 of pavement cells, chloride cells and hatching gland cells in the developing branchial
690 area of the trout *Salmo trutta*. *Journal of Zooogy*, 243, 637-651.

691 Roubal, F. R., Lester, R. J. G., & Foster, C. K. (1989). Studies on cultured and gill-attached
692 *Paramoeba* sp. (Gymnamoebae: Paramoebidae) and the cytopathology of paramoebic
693 gill disease in Atlantic salmon, *Salmo salar* L., from Tasmania. *Journal of Fish*
694 *Diseases*, 12(5), 481–492. <http://doi.org/10.1111/j.1365-2761.1989.tb00559.x>

695 Sardella, B., Matey, V., Cooper, J., Gonzalez, R. and Brauner, C. (2004). Physiological,
696 biochemical and morphological indicators of osmoregulatory stress in ‘California’
697 Mozambique tilapia (*Oreochromis mossambicus* × *O. urolepis hornorum*) exposed to
698 hyper saline water. *Journal of Experimental Biology*, 207, 1399–1413.

699 Shinn, A. P., Pratoomyot, J., Bron, J. E., Paladini, G., Brooker, E. E., & Brooker, A. J.
700 (2015). Economic costs of protistan and metazoan parasites to global mariculture.
701 *Parasitology*, 142, 196–270. <http://doi.org/10.1017/S0031182014001437>

702 Speare, D. J., Arsenault, G., MacNair, N., & Powell, M. D. (1997). Branchial lesions
703 associated with intermittent formalin bath treatment of Atlantic salmon, *Salmo salar* L.,
704 and rainbow trout, *Oncorhynchus mykiss* (Walbaum). *Journal of Fish Diseases*, 20(1),
705 27–33. <http://doi.org/10.1046/j.1365-2761.1997.d01-103.x>

706 Steinum, T., Kvellestad, A., Rønneberg, L. B., Nilsen, H., Asheim, A., Fjell, K., ... Dale, O.
707 B. (2008). First cases of amoebic gill disease (AGD) in Norwegian seawater farmed
708 Atlantic salmon, *Salmo salar* L., and phylogeny of the causative amoeba using 18S
709 cDNA sequences. *Journal of Fish Diseases*, 31(3), 205–214.
710 <http://doi.org/10.1111/j.1365-2761.2007.00893.x>

711 Taylor, R. S., Kube, P. D., Muller, W. J., & Elliott, N. G. (2009). Genetic variation of gross
712 gill pathology and survival of Atlantic salmon (*Salmo salar* L.) during natural amoebic
713 gill disease challenge. *Aquaculture*, 294(3–4), 172–179.
714 <http://doi.org/10.1016/j.aquaculture.2009.06.007>

715 Taylor, R. S., Muller, W. J., Cook, M. T., Kube, P. D., & Elliott, N. G. (2009). Gill
716 observations in Atlantic salmon (*Salmo salar*, L.) during repeated amoebic gill disease
717 (AGD) field exposure and survival challenge. *Aquaculture*, 290 (1–2), 1–8.
718 <http://doi.org/10.1016/j.aquaculture.2009.01.030>

719 Van Der Heijden, A. J. H., Van Der Meij, J. C. A., Flik, G., & Wendelaar Bonga, S. E.
720 (1999). Ultrastructure and distribution dynamics of chloride cells in tilapia larvae in
721 fresh water and sea water. *Cell and Tissue Research*, 297(1), 119–130.
722 <http://doi.org/10.1007/s004410051339>

723 Wendelaar Bonga, S.E. and van der Meij, J.C.A. (1989). Degeneration and death by
724 apoptosis and necrosis of the pavement and chloride cells in the gills of the teleost.
725 *Cell Tissue Research*, 255, 235–243.

726 Wendelaar Bonga, S.E., Flik, G., Balm, P.H.M. and van der Meij, J.C.A. (1990). The
727 ultrastructure of chloride cells in the gills of the teleost *Oreochromis mossambicus*
728 during exposure to acidified water. *Cell Tissue Res.* 259 (575–585).
729

730 Wilson, J. M., & Laurent, P. (2002). Fish gill morphology: Inside out. *Journal of*

731 *Experimental Zoology*, 293(3), 192–213. <http://doi.org/10.1002/jez.10124>

732 Young, N. D., Crosbie, P. B. B., Adams, M. B., Nowak, B. F., & Morrison, R. N. (2007).

733 *Neoparamoeba perurans* n. sp., an agent of amoebic gill disease of Atlantic salmon

734 (*Salmo salar*). *International Journal for Parasitology*, 37(13), 1469–1481.

735 <http://doi.org/10.1016/j.ijpara.2007.04.018>

Figure legends

Figure 1. Histology of AGD infected Atlantic salmon gills following cohabitation challenge.

A) Section of gills from infected Atlantic salmon from Group D (gross gill score: 1.0-1.5). An example of focal basal hyperplasia occupying <50% of the length of the secondary lamellae (upper box) and distal lamellar fusion occupying < 50% lamellae of the length of the secondary lamellae (lower box) (bar = 50µm); B) Higher magnification of A) (upper box). *Note* the formation of intercellular oedema (OE) (asterisks) (bar = 10µm); C) Higher magnification of A) (lower box). *Note* formation of lacunae (L) (bar = 10µm); D) Section of gills from infected Atlantic salmon from Group C (gross gill score: 0.5-1.0). An example of a medium focal lesion involving more than three lamellae and extending > 50% of lamellae length (bar = 50µm). Insert; higher magnification of boxed area. The lesion involves multiple epithelial cells undergoing hydropic degeneration and extensive areas of intercellular oedema (asterisks) contributing to the disruption of the lesion surface (bar = 20µm); (E) Section of gill from infected Atlantic salmon from Group E (gross gill score: 3.5-4.5). An example of a locally extensive lesion illustrating the total loss of normal gill architecture. The presence of *Neoparamoebae* sp. associated with the sloughing epithelium (arrows) (bar = 500µm); F) Section of histologically normal gill from Atlantic salmon from Group A (bar = 500µm).

Figure 2. Quantification and qualification of lesions in AGD infected gills tissue of Atlantic salmon. Group A: clear; Group B: very light; gross gill score 0-0.5, Group C: light; gross gill score 0.5-1, Group D: very mild; gross gill score 1-1.5; Group E: heavy; gross gill score 3.5 – 4.5 (n = 3 per group). There is a positive link between gross gill scores and the number and severity of the lesions in the low-grade AGD groups. In the heavy infection level category

(Group E), lesions were much reduced in number due to the larger surface area exhibited by the more severe lesions.

Figure 3. Immunohistochemistry of AGD-affected Atlantic salmon gills following cohabitation challenge showing immunolabeled chloride cells within ‘small focal’ lesions. Micrographs B-F are from gills of AGD infected fish from Group D exhibiting gross gill scores of 1-1.5. A) Localised Na^+/K^+ -ATPase immunolabeling of normal chloride cells from a Group A fish. The positive immunolabeled cells are predominately distributed on interlamellar regions. A few chloride cells were also noted along the lamellae (arrow) (bar = 50 μm); B) Absence of Na^+/K^+ -ATPase immunolabeling at interlamellar regions of lesion site where minimal basal lamellar hyperplasia was detected (arrowheads). Visible intra-epithelial oedema at the areas where the chloride cells were previously located (OE) (arrows) (bar = 50 μm); C) Hyperplastic areas demonstrating the formation of intra-epithelial oedema where the chloride cells were previously located (arrows) (bar= 50 μm); D) The hyperplastic region can be seen to extend to the neighbouring inter-lamellar space (arrows) due to a more pronounced basal lamellar hyperplasia. Note the complete loss of immunolabeled chloride cells occurring at the centre of lesions (asterisk) (bar = 50 μm); E) With more pronounced hyperplasia, the reduction in number of immunolabeled chloride cells extends to the neighbouring hyperplastic interlamellar space. Note the sloughing chloride cell (arrow) (bar = 50 μm); F) Inter and intracellular oedema (OE) (arrows) and sloughing chloride cell (arrowhead) at the surface of the hyperplastic region (bar = 50 μm).

Figure 4. Immunohistochemistry of AGD-affected Atlantic salmon gill following cohabitation challenge showing immunolabeled chloride cell within ‘small focal’, ‘medium focal’ and ‘locally extensive’ lesions. Micrographs A-C are from gills of AGD infected fish

from Group D exhibiting gross gill scores of 1-1.5 and micrograph D is from gills of AGD infected fish from Group E exhibiting gross gill scores of 3.5-4.5. A) An example of a 'medium focal' lesion. Basal hyperplasia has resulted in almost complete fusion of the lamellae with resulting lack of immunolabeled chloride cells at the lesion site. Note the distal location of chloride cells on periphery of hyperplastic regions (asterisk) (bar = 50 μ m); B) An example of a mixed 'small focal' lesion involving both basal lamellar hyperplasia and distal lamellar hypertrophy. Note the formation of the lacunae (L) (bar = 50 μ m); C) Extensive lack of immunoreactivity throughout the 'medium focal' lesion. Note sparse distribution of immunolabeled chloride cells at the edge of the lesion (arrows) (bar = 50 μ m); D) An example of a 'locally extensive' lesion showing a few isolated, immunolabeled, hypertrophic chloride cells (arrows) within the filament which is markedly expanded by epithelial hyperplasia (bar = 50 μ m).

Figure 5. Transmission Electron Micrographs of Atlantic salmon gill filaments of Group A fish (clear). A) A multi-cellular complex consisting of central chloride cell (CC) with adjacent accessory cells (AC). Normal chloride cell structure is characterised by a columnar appearance with microridges (MR) present on the apical surface, a high mitochondrial density (M) and an extensive vesicular tubular network (T) (bar = 2 μ m); B) An interlamellar space showing microridges (MR), an epithelial pavement cell (PVC), a mucous cell (MC) and chloride cells (CC) (bar = 2 μ m); C) Higher magnification of the apical portion of a chloride cell, where vesicles (V) and shorter tubules (TS) replace the more extensive intricate vesicular tubular network of the basolateral portion (bar = 390nm); D) Higher magnification of the basolateral portion of a chloride cell. Mitochondria (M), characterised by a double-membraned envelope and an electron dense matrix which containing infoldings of cristae (C),

are surrounded by well-developed vesicular tubular network in close association with the endoplasmic reticulum (ER) (bar = 290nm).

Figure 6. Transmission electron micrographs of Atlantic salmon gill filaments from Group D fish (gross gill score 1-1.5). A) Degenerative changes of a secondary lamella; areas of mild hyperplasia (arrowheads) include chloride cells (CC) and epithelial pavement cells (PVC) displaying vacuole formation within the cells and oedema (OE) at the space between lamellar epithelial cells and the basement membrane, resulting in separation of the epithelial cells from the basement membrane (arrow). Note pillar cells (PC) and intraluminal red blood cells (RBC) (bar = 5 μ m); B) An example of chloride cell degeneration; a swollen and vacuolated cell undergoing hydropic degeneration. The cytoplasm is pale due to swelling of intracellular organelle structures *i.e.* vesicular tubular system and electron dense mitochondria. The nucleus (N) is also pale. The microridges are intact but there is evidence of areas of fusion (FMR) (bar = 2 μ m); C) Micrograph showing the complete loss (arrow) and fusion (arrowheads) of microridges. A large vacuole (V) has formed in the cytoplasm due to hydropic degenerative changes (bar = 2 μ m); D) A higher magnification of cytoplasm of a degenerating CC showing oedema (OE) and swelling of the mitochondria (M); both the loss of electron density of the matrix and the loss of cristae is observed. Swelling and disorganization of the vesicular tubular network is evident (bar = 290nm).

Figure 7. Graph showing increasing *N. perurans* loads with increasing AGD gross gill scores in Atlantic salmon gills, expressed as *N. perurans* genomic equivalents 50ng⁻¹ total DNA. Group A (clear; gross gill score: 0); Group B (very light, gross gill score: 0-0.5); Group C

(light; gross gill score: 0.5-1.0); Group D (very mild; gross gill score: 1.0-1.5); Group E (heavy; from archival sample; gross gill score: 3.5-4.5). Sample type L = taken from area of visible lesion; N = taken from area with no visible lesion. Groups B-D; L samples (n = 5 per group except Group D which was n = 4) and N samples (n = 5 per group except Group D which was n = 4). Group A samples consisted of pooled biopsies taken from 2 different sites on the gill (n = 5). Group E was a single sample taken from a visible lesion (n = 5). Values are expressed as mean \pm SE. Letters on graph indicate values that were significantly different (Mann Whitney-U, $p < 0.05$).

Figure 8. Graph showing relative real-time qPCR quantification of Na⁺/K⁺-ATPase gene expression. Na⁺/K⁺-ATPase gene expression was calibrated relative to fish from Group A (clear). Values are expressed as mean \pm SE. Letters on graph indicate values that were significantly different (parametric general linear model, $p = < 0.0001$).

1 **Table 1**

2 Categorised groups corresponding to infection level category of amoebic gill disease and the
3 corresponding gill score (Taylor, Muller, Cook, Kube, & Elliott, 2009) of fish from the current
4 study.

5

Group	Infection level category	Gross AGD gill score
A	Clear	0
B	Very light	0 – 0.5
C	Light	0.5 - 1
D	Very mild	1 – 1.5
E†	Heavy	3.5 – 4.5

6

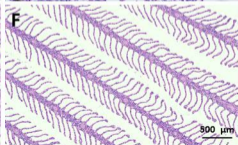
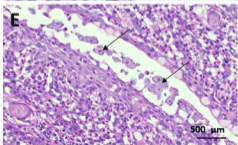
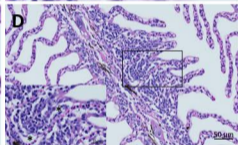
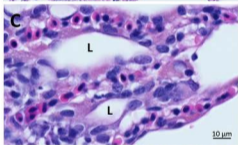
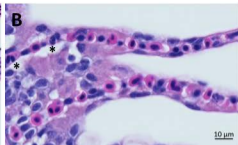
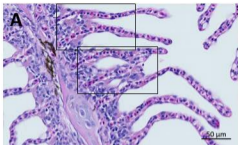
7 † refers to archival samples.

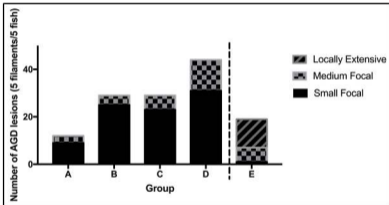
1 **Table 2** qPCR primers sequence for Na⁺/K⁺-ATPase gene expression analysis

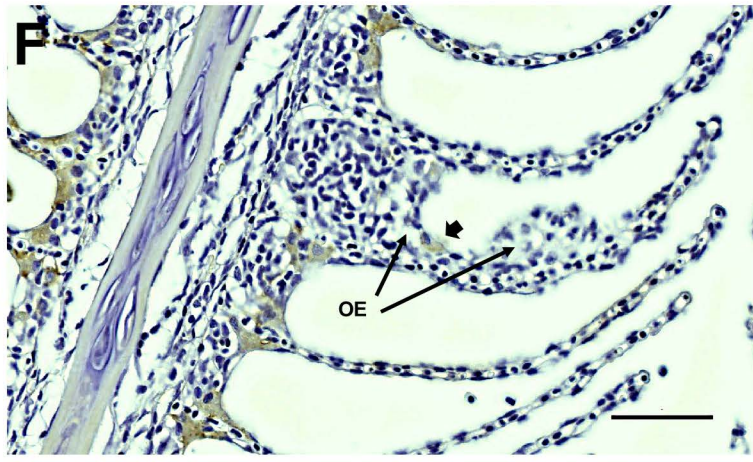
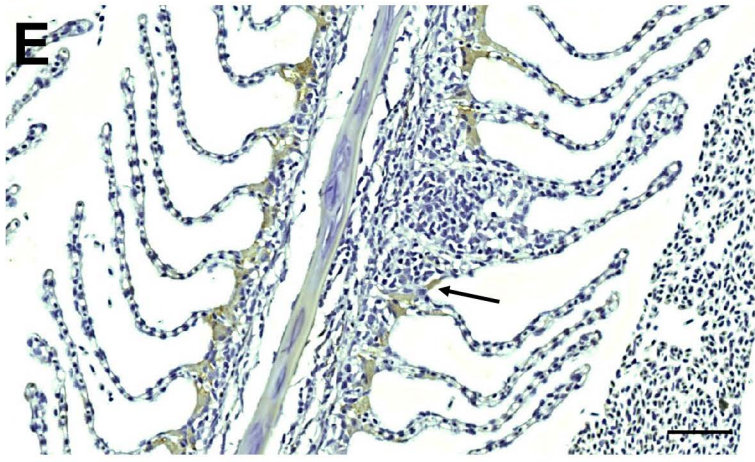
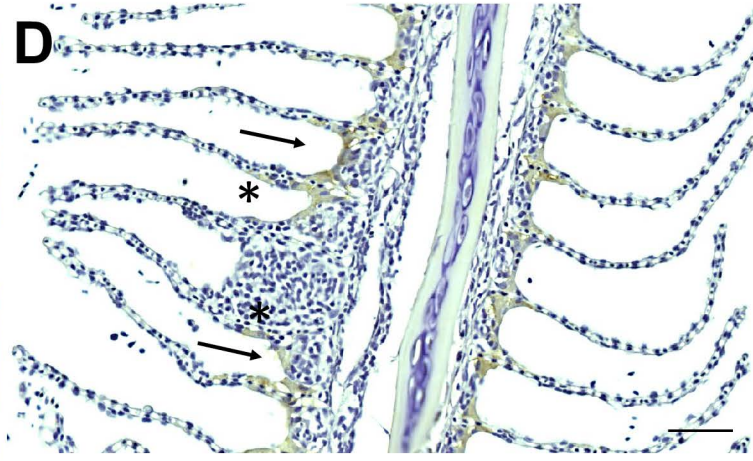
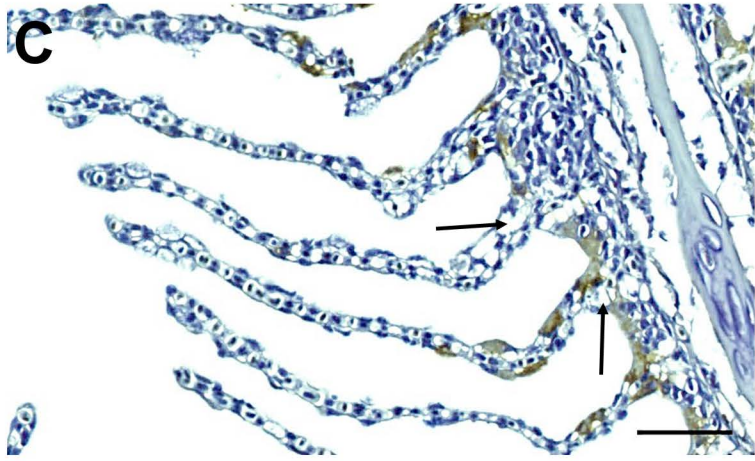
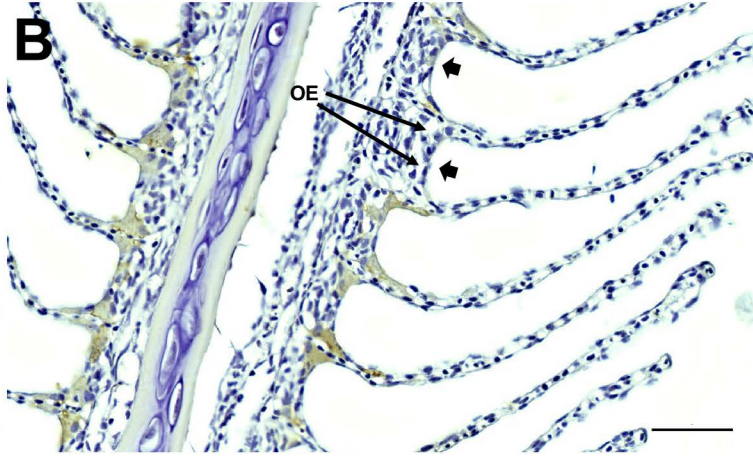
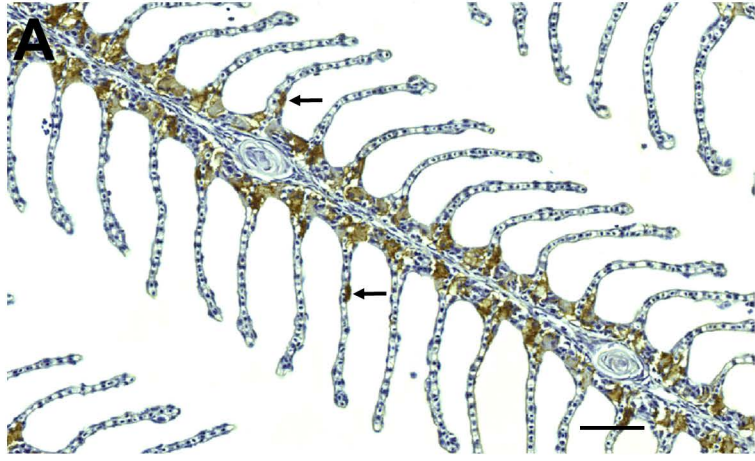
2

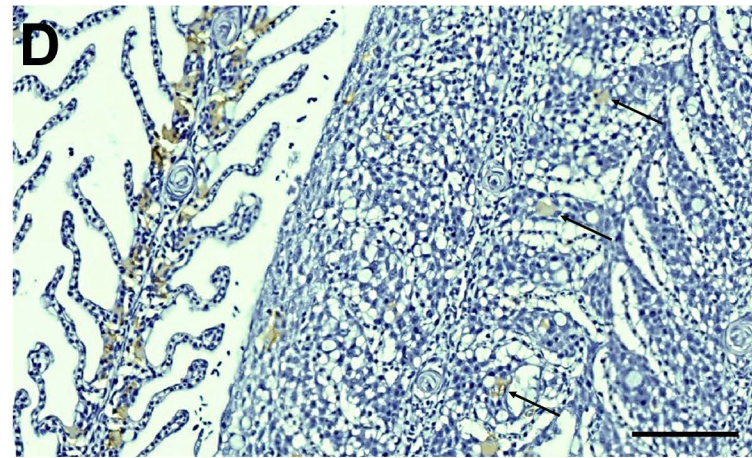
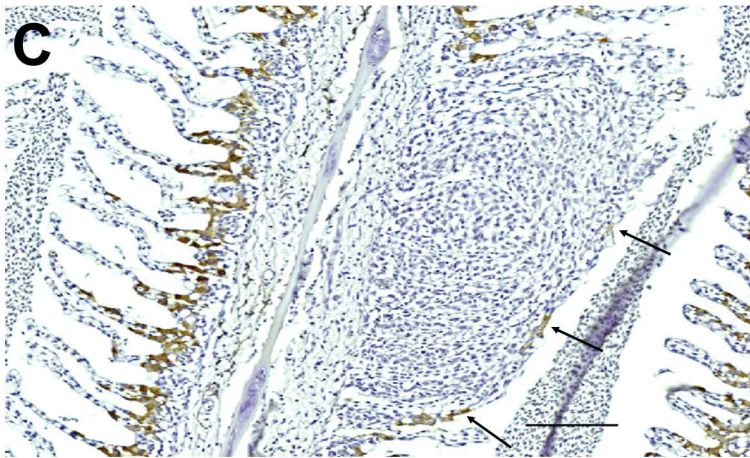
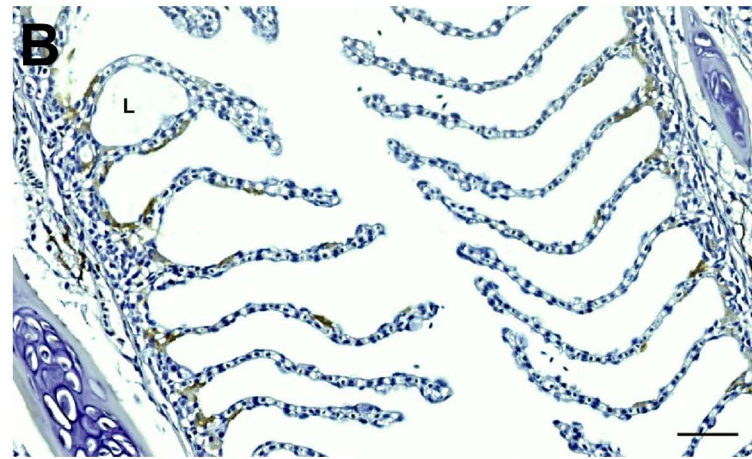
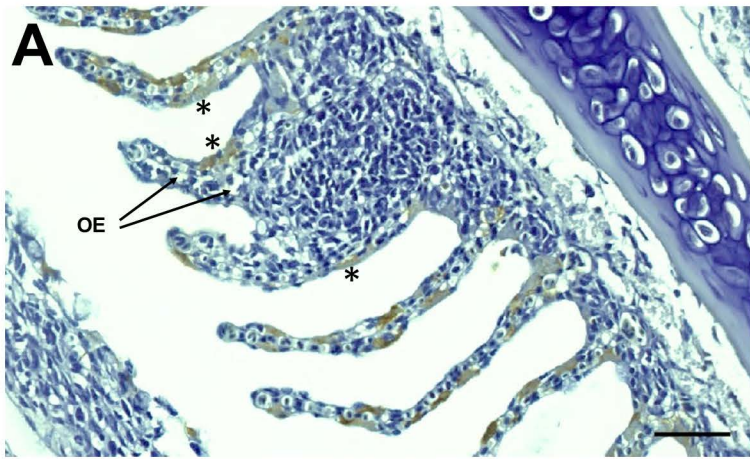
Transcript	Primer Name	Primer sequence	Efficiency	Source
Target Genes				
Na ⁺ /K ⁺ -ATPase	As_NaK_β1_F	CCAATGAAAGCATCCCTAG	0.99	Madsen, Kiilerich, & Tipsmark (2009)
	As_Nak_β1_R	GGCGTCCTCCTCTCTCTTGT		
Reference Genes				
ELF-1	As_ELF1_F	CTGCCCCTCCAGGACGTTTACAA	0.99	Morais, Monroig, Zheng, Leaver, & Tocher (2009)
	As_ELF1_R	CACCGGGCATAGCCGATTCC		
Cofilin-2	As_Cofilin2_F	AGCCTATGACCAACCCACTG	0.97	Herath, Bron, Thompson, Taggart, Adams, Ireland, & Richards, (2012)
	As_Cofilin2_R	TGTTACACAGCTCGTTTACCG		
β actin	As_actin_F	ACTGGGACGACATGGAG	0.96	Morais Monroig, Zheng, Leaver, & Tocher (2009)
	As_actin_R	GGGGTGTTGAAGGTCTC		

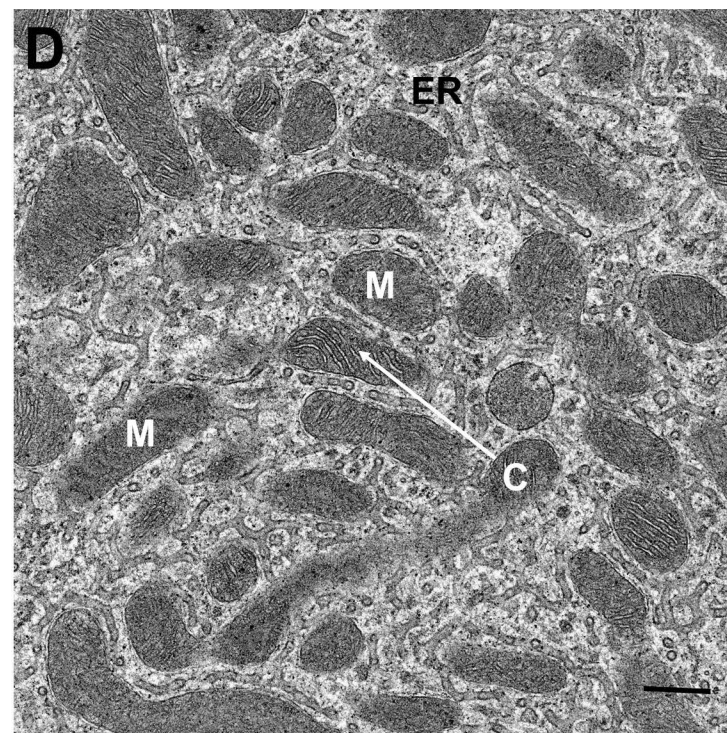
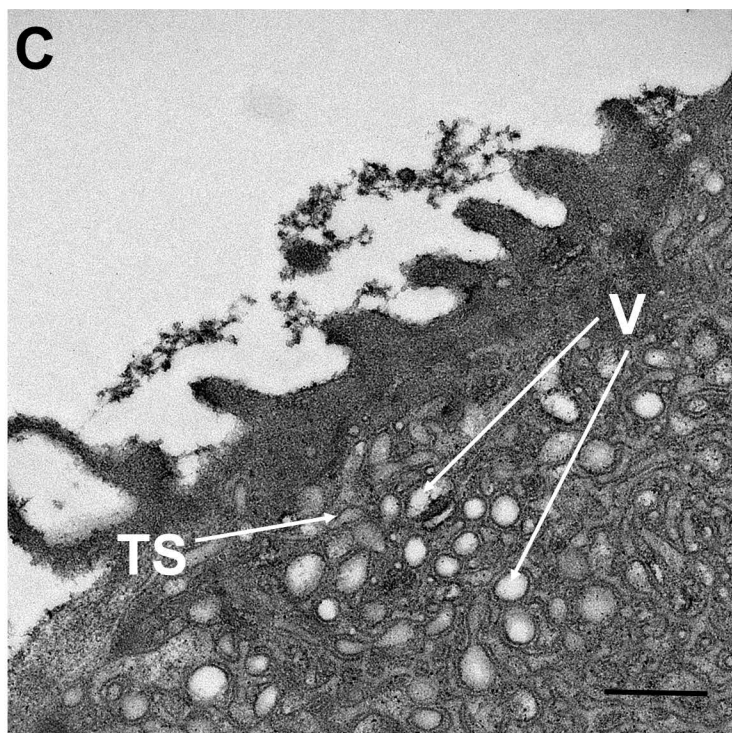
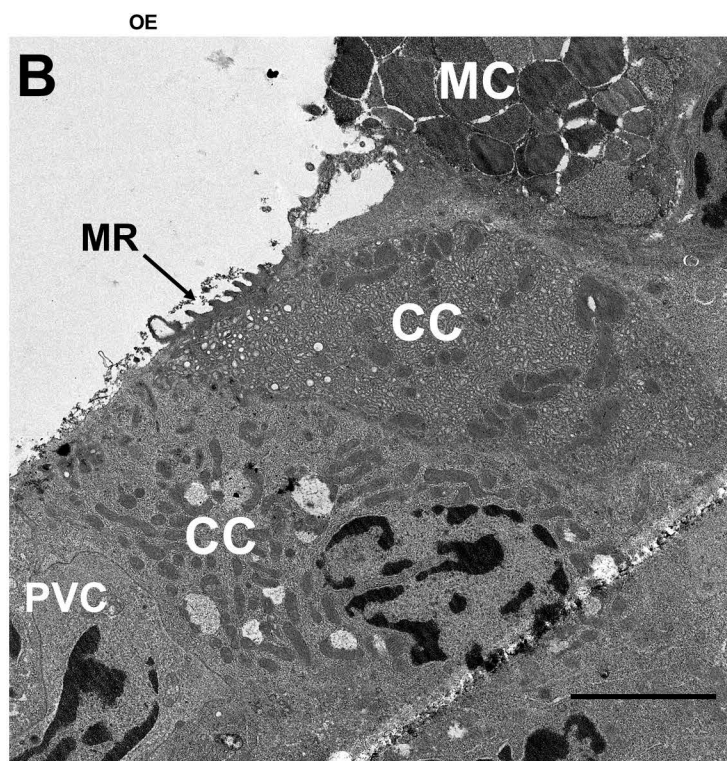
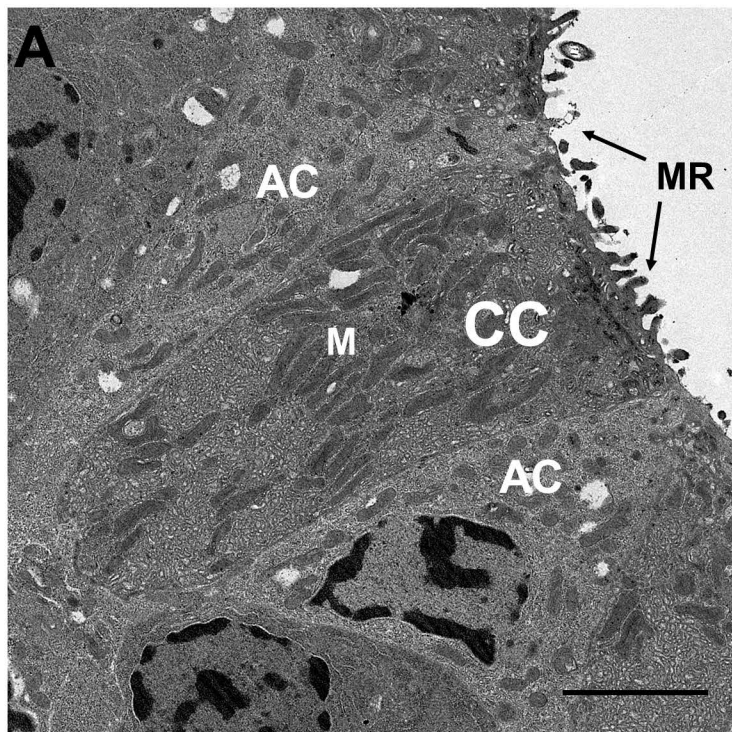
3

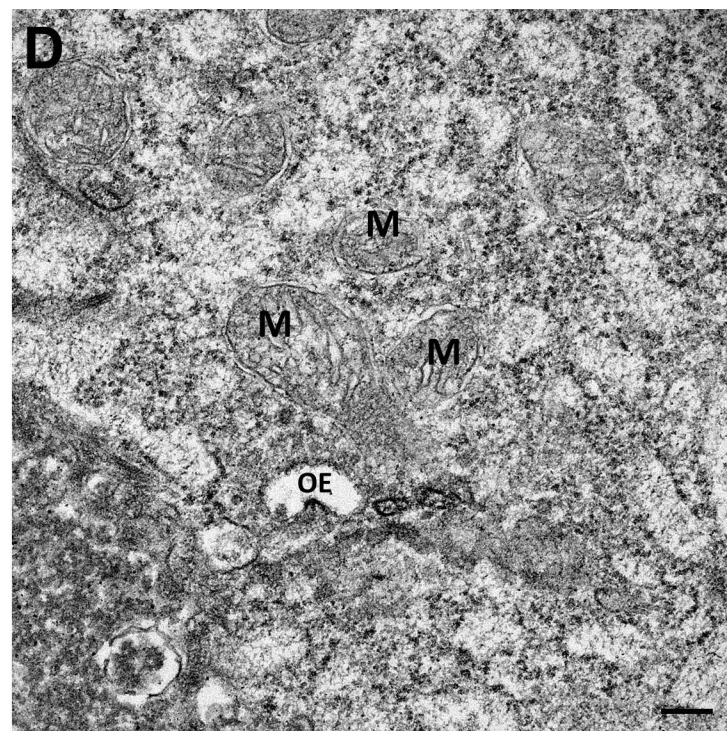
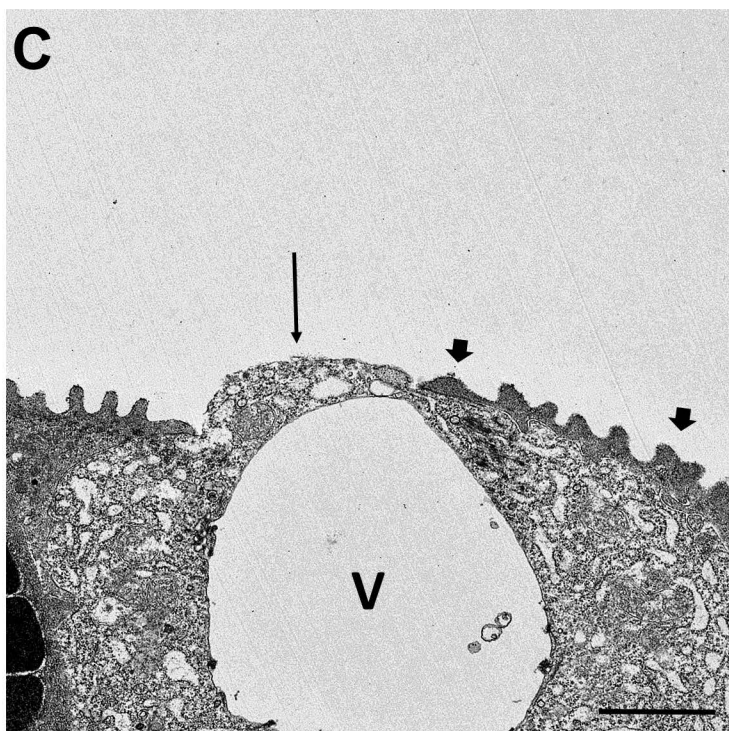
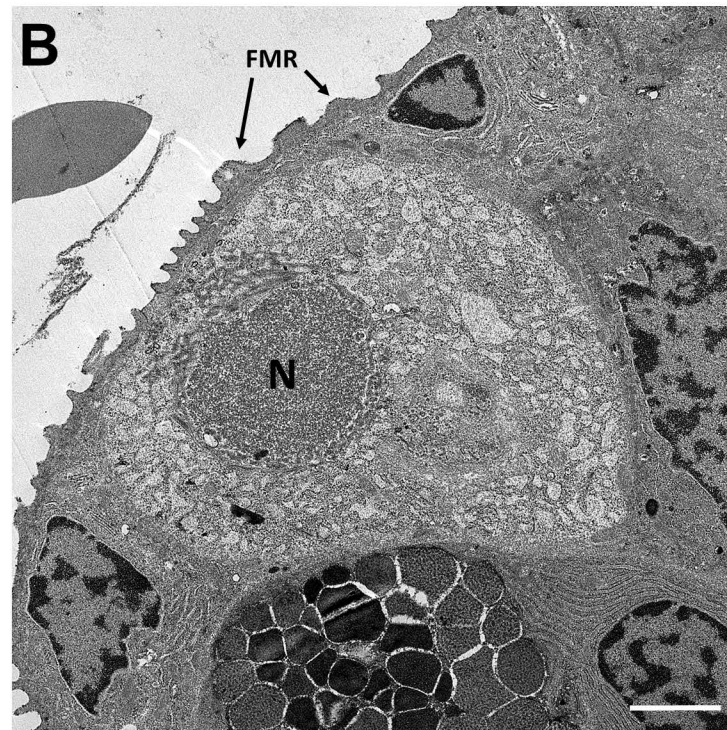
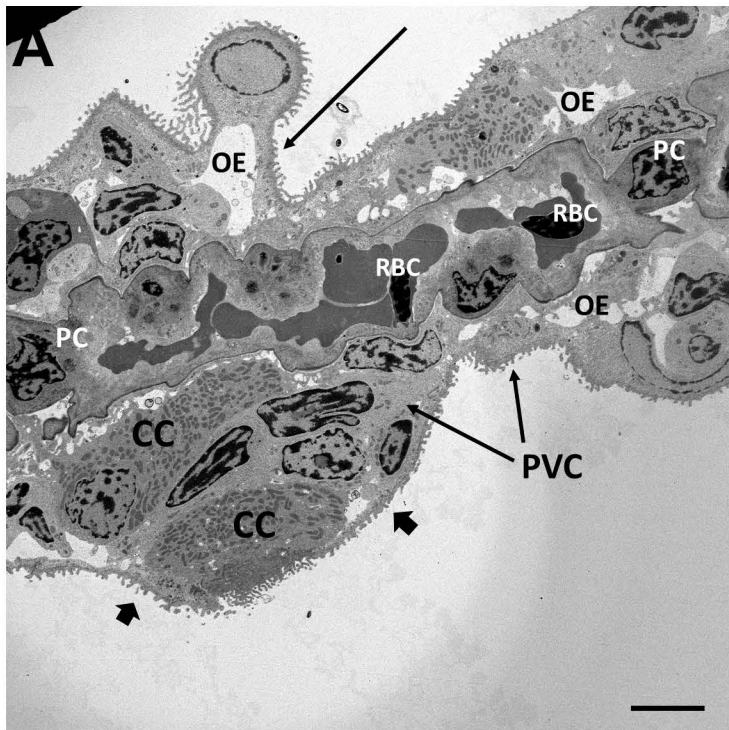


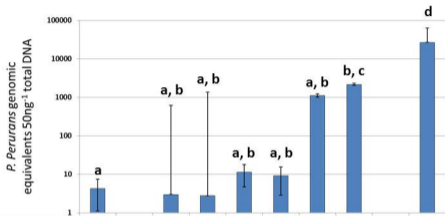




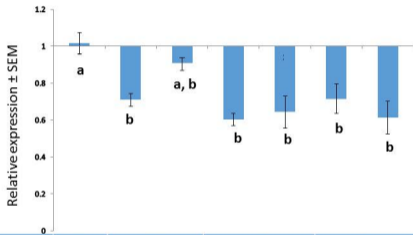








Group	A	B		C		D		E
Gill score	0	0-0.5		0.5-1		1-1.5		3.5-4.5
Sample type	-	L	N	L	N	L	N	L



Group	A	B	C	D
Gill score	0	0-0.5	0.5-1	1-1.5
Sample type	-	L N	L N	L N